Nuclear photoproduction of vector mesons within a Monte Carlo approach

I. González*
Instituto de Física, Universidad de São Paulo, São Paulo, Brasil
and Instituto Superior de Tecnologías y Ciencias Aplicadas, Havana, Cuba

F. Guzmán†
Instituto Superior de Tecnologías y Ciencias Aplicadas, Havana, Cuba

A. Deppman‡
Instituto de Física, Universidad de São Paulo, São Paulo, Brasil

(Received 19 February 2014; revised manuscript received 2 April 2014; published 21 May 2014)

We present recent improvements in the CRISP code for nuclear reaction simulation. The photoproduction of vector mesons was included in the code, which can evaluate also final state interaction of these mesons with the nucleus. Effects such as shadowing, subthreshold production, and Pauli blocking can be observed. The model is described in detail and some important quantities, such as cross section and nuclear transparency, are calculated as examples of the potential of our code.

DOI: 10.1103/PhysRevC.89.054613 PACS number(s): 24.10.Lx, 25.20.Lj

I. INTRODUCTION

Photon induced reactions are important tools to investigate nuclear and nucleonic structures. The photoabsorption process allows the study of the formation and propagation of several particles inside nuclear matter, such as baryonic resonances and hyperons [1–6]. It is also useful to observe the shadowing effect in the photoabsorption cross section, which is the result of the hadronization process of photons in the nuclear medium. Photonuclear reactions are characterized by their remarkable simplicity, since they do not produce strong modifications in the nuclear structures compared to those induced by strongly interacting particles. These features make the photonuclear reaction very attractive for the study of nuclear and subnuclear structure.

Photonuclear reactions above 1 GeV exhibit a process completely different from those in the region covering baryonic resonances. Above this energy region, the photon presents a hadronic component in its wave function that considerably increases the cross section of the nucleons. According to vector dominance models (VDMs) [7,8], in complex nuclei, the photoabsorption cross section is dominated by the interaction of a bound state $(q\bar{q})^{J=1}$, known as vector meson. The study of photonuclear production of vector mesons allows the investigation of possible modification of mesons and barions in the presence of nuclear matter. Experiments at the HERA electron-proton collider have also found evidences of light vector meson production at large virtuality Q^2 and heavy $q\bar{q}$ vector mesons at all Q^2 [9,10]. Combined analysis of inclusive deep-inelastic scattering and hard vector meson production may substantially improve our understanding of strong interactions at high energies. At the same time, the properties of particles generated on the nuclear medium, such as the modification of the hadron mass, allow the study of strong interaction phenomena in the perturbative quantum chromodynamics (QCD) regime. Some of these of nuclear reactions are currently under study at the Large Hadron Collider (LHC) and Thomas Jefferson Accelerator Facility (JLab)[11–18].

Intermediate and high energy nuclear reactions are complex processes involving many-body interactions. The most effective approach to this problem is the Monte Carlo (MC) method that has been successfully implemented in several codes. Some of the oldest and best known codes for intranuclear cascade and/or nuclear evaporation are Bertini's model [19], the ISABEL intranuclear cascade (INC) [20,21], and the codes developed by Barashenkov and collaborators [22–25]. There are many versions of these codes reflecting improvements along time, and many interesting results have been obtained [13,26–34]. However, these codes consider the intranuclear cascade as a sequence of individual particle events along their tracks within the unphysical hypothesis that all the other particles inside the nucleus may be treated as static objects. In the last thirty years, with the enhancement of computational power, new multicollisional methods for the intranuclear cascade have been developed [35–38], providing a time-ordered evolution of the cascade by taking into account the nucleus configuration at each instant of time. These methods introduce a more realistic description of the intranuclear cascade, the Pauli blocking mechanism, and the density fluctuation, resulting in a more precise description of nuclear processes. These codes have produced results in good agreement with a larger set of experimental data, using a smaller number of parameters. A discussion about the advantage of these improved codes with respect to the older codes can be find in Ref. [39–41].

The CRISP code [41], which has been developed during the last 25 years, is a combination of Monte Carlo (MC) and quantum molecular dynamics (QMD) methods. CRISP allows the study of several aspects of nuclear reactions such as fission

*israel@if.usp.br
†guzman@instec.cu
‡adeppman@gmail.com

and spallations cross sections, mass and/or atomic number distributions of nuclear fragments produced during reactions, and multiplicity of secondary particles. Also some nuclear mechanisms which would be difficult to study experimentally can be investigated with the CRISP code, such as the Pauli blocking. This mechanism causes some processes that could be observed in vacuum may not be allowed in the nuclear environment.

In the present work we show new developments in the CRISP code obtained by introducing the photoproduction of vector mesons. These developments are represented by the inclusion of vector meson production through the VDM approach and the inclusion of the final state interaction (FSI) of those vector mesons with nucleons. A comprehensive analysis of this implementation is performed by reproducing large set of experimental data from photonuclear production of vector-meson experiments.

After analyzing the implementation itself, we use the code for the study of some selected aspects in the photoproduction of vector mesons. It is not our objective here to give a detailed analysis of the production of each vector meson, but mainly to show that the CRISP code now provides an excellent tool for the study of the nuclear process following the vector meson production. Some of these processes addressed here are Pauli blocking, Fermi motion, the shadowing effect, and subthreshold photoproduction.

The paper is organized as follows. In Sec. II we discuss the methodology for the inclusion of the vector-meson photoproduction. In Sec. III we present our results and discuss them in comparison with experimental data and give some examples of study of the nuclear processes which follow the vector-meson production in nuclei. In Sec. IV we present our conclusions.

II. METHODOLOGY

At intermediate energies, it is assumed that nuclear reactions take place at two main stages. The first corresponds to a multicollisional dynamics of nucleons triggered by an incoming energetic particle transferring energy and momentum. This process lead to the production of several light particles and a residual nucleus in a statistical equilibrium. The second stage of the reaction is characterized by the decay of this residual nucleus emitting nucleons or a cluster of nucleons. At high energies, also the multifragmentation process, where the nucleus breaks up, can take place.

The CRISP package [41] is C++ software able to perform nuclear reactions induced by several probes. It describes the two steps of nuclear reactions: (1) the intranuclear cascade using a multicollisional approach and (2) the competition between particle evaporation and fission processes by Monte Carlo methods. The code presents several features, such as (i) the excitation of nucleonic resonances heavier than the Δ resonances, (ii) the initial nuclear ground-state construction according to the Fermi model and Pauli principle, (iii) the quasideuteron channel for photoabsorption, (iv) a more realistic parameter-free Pauli blocking mechanism, and (v) a parameter-free energetic cascade stopping criterion. The nuclear dynamics is considered [37,42] in a nucleus modeled by an infinite square potential. The effects of the nuclear potential are presented in the transmission of the particles through the nuclear surface or through the effective mass approximation [43]. The multicollisional calculation is accomplished by constantly updating all the kinematics variables of all particles inside the nucleus, which make it possible to study more realistically many nuclear phenomena.

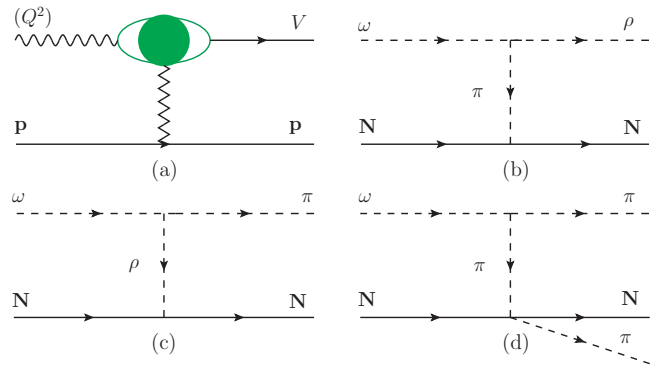

FIG. 1. (Color online) The Feynman diagrams for photoproduction of vector mesons (a) and ωN final state interactions (b)–(d) included in CRISP code.

Every process in CRISP code is ruled by the Pauli blocking mechanism that results from the antisymmetrization of the nuclear wave function. The Pauli exclusion principle is taken into account in CRISP dynamics by rejecting collisions that lead to the final state violating the Pauli principle. All these features enabled CRISP code to successfully simulate reactions induced by protons [40,44], photons [39,41,45,46], electrons [47,48], and other processes such as kaon [49] production and hypernuclei decay [50–52]. The effectiveness of such an approach can be verified in the study of evaporation/fission competition [53–55], which explained for the first time the saturation below the unit of fissility for heavy nuclei observed in experiments. Also, good results have been obtained in the study of the production of intermediate mass fragments (IMFs) induced by protons [56].

For the extension of applicability of the CRISP to high energies we've added the photoproduction of vector mesons ρ, ω, ϕ, and J/Ψ and their interactions with nucleons. The photoproduction process is shown in diagram (a) of Fig. 1, while diagrams (b), (c), and (d) represent ρ, ω, and ϕ interactions with nucleons by one-meson exchange. The diagrams of Fig. 2 represent the J/Ψ vector meson interaction with nucleons by one-boson exchange. Also, a resonant model is used for other ρ, ω, and ϕ interactions with nucleons and they are represented by the diagrams shown in Fig. 3. We explain in detail the main features of these models in the next sections.

A. The photoproduction process of vector mesons

The process of photoproduction of vector mesons is considered in the soft dipole Pomeron universal model proposed by Martynov, Predazzi and Prokudin [57]. In this model the Pomeron is a double Regge pole with an intercept equal to 1, so the Froissart-Martin bound [58] is not violated. With this model it is possible to reproduce all photoproduction data

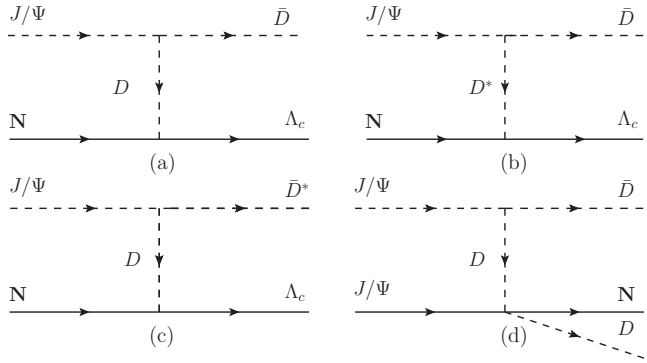

FIG. 2. The Feynman diagrams for J/Ψ dissociation included in CRISP code.

for ρ, ω, ϕ, and J/Ψ mesons and to predict the behavior of Υ in the energy region $1.7 \leqslant W \leqslant 250$ GeV, at values of photon virtualities $0 \leqslant Q^2 \leqslant 35$ GeV^2 and for values of the transfered four-momentum $|t| < 1.6$ GeV. The application of the soft dipole Pomeron exchange model [59] is supported by J/Ψ photoproduction experiments using the ZEUS detector [60], that suggest a soft process to describe the photoreaction instead of a pure QCD process.

It is assumed that a photon state fluctuates into a quark-antiquark pair with lifetime determined by the uncertainty principle as $2\nu/(Q^2 + M_V^2)$, where ν is the beam energy. This large lifetime allows protons to interact with the quark-antiquark pair via Pomeron or secondary Reggeon exchange, producing a vector meson. The Feynman diagram of photoproduction of a vector meson via Pomeron exchange is shown in diagram (a) of Fig. 1.

In the VMD model, the amplitude of the photoreaction is related to the vector meson–nucleon scattering process as

$$A_{\gamma p \to Vp} = N_C N_V A_{Vp \to Vp}, \tag{1}$$

where the coefficients N_C and N_V can be found from relationships using e^- e^+ decay widths of vector mesons assuming SU(4) flavor symmetry [57]. The vector meson–nucleon scattering amplitude is given by [57]

$$A\left(z,t,M_V^2,\tilde{Q}^2\right) = \mathbb{P}\left(z,t,M_V^2,\tilde{Q}^2\right) + f\left(z,t,M_V^2,\tilde{Q}^2\right) + \cdots, \tag{2}$$

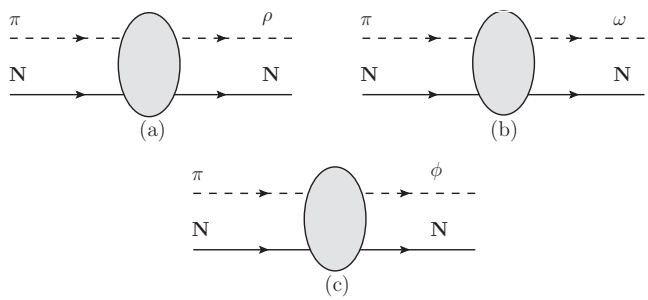

FIG. 3. The diagrams for resonant process of π final state interactions producing ρ, ω, and ϕ mesons included in CRISP code.

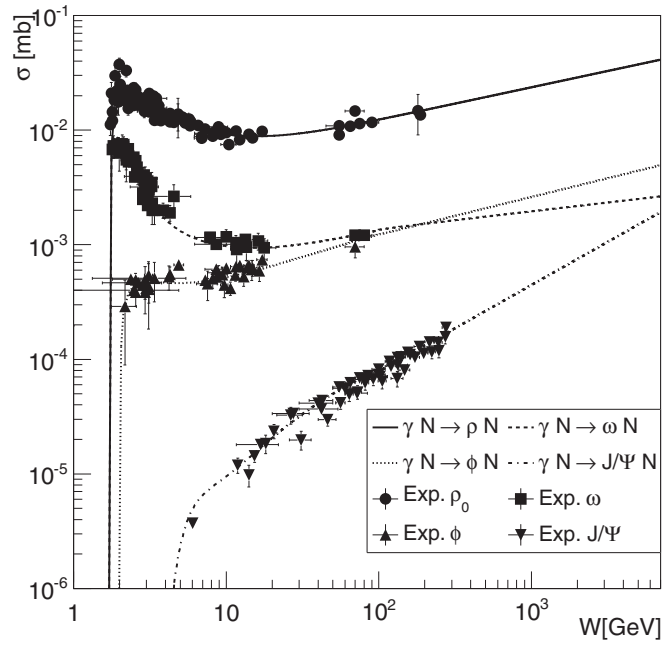

FIG. 4. Elastic cross sections for vector meson photoproduction for proton from the threshold to high energies.

where $\tilde{Q}^2 = M_V^2 + Q^2$. $\mathbb{P}(z,t,M_V^2,\tilde{Q}^2)$ is the Pomeron contribution given by [57]

$$\mathbb{P}\left(z,t,M_V^2,\tilde{Q}^2\right) = ig_0\left(t,M_V^2,\tilde{Q}^2\right)(-iz)^{\alpha_{\mathbb{P}}(t)-1} + ig_1\left(t,M_V^2,\tilde{Q}^2\right)\ln(-iz)(-iz)^{\alpha_{\mathbb{P}}(t)-1}. \tag{3}$$

Here the first term is a single j pole contribution and the second is the contribution of the double j pole. The second term at the right-hand side of Eq. (2) corresponds to the f-Reggeon contribuition and is given by [57]

$$f\left(z,t,M_V^2,\tilde{Q}^2\right) = ig_f\left(t,M_V^2,\tilde{Q}^2\right)(-iz)^{\alpha_f(t)-1}. \tag{4}$$

The model includes 12 free parameters defined by fitting 357 experimental data points for each meson. This fit results in a quite satisfactory agreement, even to data near threshold, as shown in Fig. 4.

The differential and total cross section for $Vp \to Vp$ process are given by

$$\frac{d\sigma}{dt} = 4\pi\left|A_{Vp\to Vp}\left(z,t,M_V^2,\tilde{Q}^2\right)\right|^2, \tag{5}$$

$$\sigma\left(z,M_V^2,\tilde{Q}^2\right)_{el}^{\gamma p\to Vp} = 4\pi\int_{t_-}^{t_+} dt\left|A_{Vp\to Vp}\left(z,t,M_V^2,\tilde{Q}^2\right)\right|^2, \tag{6}$$

t_+ and t_- being the transferred momenta determined by the kinematical condition $-1 \leqslant \cos\theta_s \leqslant 1$, where θ_s is the scattering angle in the s channel of the reaction. Equation (6) reproduces experimental data from threshold up to 250 GeV. These are the issues concerning the model proposed by Martynov *et al.* For further details, refers to the original article [57].

At higher energies the cross section $\sigma(\gamma p \to Vp)$ can be parametrized in a simpler way as [61]

$$\sigma(\gamma p \to Vp)_{\rho,\omega} = b_v(XW^{\varepsilon} + YW^{\eta}), \tag{7}$$

$$\sigma(\gamma p \to Vp)_{\phi,J/\Psi} = b_v(XW^{\varepsilon}). \tag{8}$$

where W is the center-of-mass energy. The terms with X and Y correspond to Pomeron and meson exchange contributions to the cross section, respectively. In the case of the mesons ϕ and J/Ψ the meson exchange term is suppressed, leaving only the Pomeron exchange [61].

We have fitted Eqs. (7) and (8) to experimental data at center of mass energies far from threshold (40 GeV) and obtained the, where σ is given in μb and W in GeV:

$$\begin{aligned}
\sigma_{\gamma N\to\rho N} &= 3.31\, W^{0.28} + 173.40\, W^{-1.66},\\
\sigma_{\gamma N\to\omega N} &= 0.67\, W^{0.15} - 5901.63\, W^{-2.70},\\
\sigma_{\gamma N\to\phi N} &= 0.27\, W^{0.33},\\
\sigma_{\gamma N\to J/\Psi N} &= 0.0024\, W^{0.75}.
\end{aligned} \tag{9}$$

These fits allow us to extend the energy range of the photoproduction of vector mesons up to center-of-mass energies of a few TeV.

The vector meson photoproduction cross section can now be calculated with the CRISP code. In Fig. 4 we report the results for the photoproduction of ρ, ω, ϕ, and J/Ψ for protons. We observe good agreement between calculation and experiments, showing that the primary interaction of the photon with the nucleon is well described. In the following we assume that the photon interaction with protons and neutrons can be described by the cross section discussed above.

B. Final state interactions

For a correct treatment of vector mesons in nuclear medium, the CRISP code incorporates meson-nucleon interaction channels for ρ, ω, ϕ, and J/Ψ mesons. For elastic reaction channels $VN \to VN$ we use the Eq. (6), while for inelastic reactions $VN \to V'N'$ we use two models: the one-meson exchange and the resonant models, as described below.

1. One meson exchange model for ρ, ω, and ϕ mesons

For $\omega N \to \pi N$, $\to \rho N$, and $\to \pi\pi N$ channels we use the one-boson exchange model (EM) proposed by Lykasov, Cassing, Sibirtsev, and Rzjanin [62] that adopts the $\omega\rho\pi$ dominance model proposed by Gell-Mann, Sharp, and Wagner [63], summarized in diagrams (b)–(d) of Fig. 1. The coupling constant $g_{\omega\rho\pi}$ and form factor are fixed by the reaction $\pi N \to \omega N$ from comparison to experimental data.

The model uses the effective Lagrangian for the exchange of meson V,

$$\mathcal{L} = \mathcal{L}_{\omega\rho\pi} + \mathcal{L}_{VNN}, \tag{10}$$

where the $\omega\rho\pi$ interaction Lagrangian is

$$\mathcal{L}_{\omega\rho\pi} = -\frac{g_{\omega\rho\pi}}{m_\omega}\epsilon_{\alpha\beta\gamma\delta}\partial^\alpha\rho^\beta\partial^\gamma\omega^\delta\pi. \tag{11}$$

The coupling constant $g_{\omega\rho\pi} = 11.79$ was evaluated from the $\omega \to 3\pi$ partial width of ω meson decay [63], $\epsilon_{\alpha\beta\gamma\delta}$ is the antisymmetric tensor, while ω, ρ, and π are the corresponding meson fields. The interaction Lagrangian for vertices πNN and ρNN are

$$\mathcal{L}_{\rho NN} = -g_{\rho NN}\left(\bar{N}\gamma^\mu\tau N\rho_\mu + \frac{\kappa}{2m_N}\bar{N}\sigma^{\mu\nu}\tau N\partial_\mu\rho_\nu\right), \tag{12}$$

$$\mathcal{L}_{\pi NN} = -g_{\pi NN}\bar{N}\gamma_5\tau N\cdot\pi, \tag{13}$$

where N stands for the nucleon field, τ for the Pauli matrices, and $g_{\rho NN} = 3.24$ is defined according to Ref. [64]. The tensor coupling constant is given by the ratio $\kappa = f_{\rho NN}/g_{\rho NN} = 6.1$, while $g_{\pi NN} = 13.59$ [65]. For further details, refers to the original article [62].

The angular distribution for two-particle collision is given using the differential cross section equation, while for the $\omega N \to \pi\pi N$ reaction we use the four-momentum phase space generator from the ROOT package [66]. This generator is based on the GENBOD function (W515 from CERNLIB) which is based on the Raubold and Lynch method [67]. We also include in our code the inverse reactions $\rho N \to \omega N$ and $\pi N \to \omega N$, which can be calculated by the detailed balance principle.

The differential cross sections obtained from the previous interaction Lagrangian written in Eq. (10) are [62]

(i) For $\pi N \to \omega N$,

$$\begin{aligned}
\frac{d\sigma}{dt} =& \frac{g^2_{\omega\rho\pi}}{m^2_\omega}\frac{1}{8\pi\lambda(s,m_N^2,m_\pi^2)}\frac{F^2_{\omega\rho\pi}F^2_{\rho NN}}{(t-m_\rho^2)^2}\\
&\times\left[-(g_{\rho NN}+f_{\rho NN})^2 m_\omega^2 q_\omega^2 t\right.\\
&+\left(g^2_{\rho NN} - \frac{f^2_{\rho NN}t}{4m_N^2}\right)\\
&\left.\times\left(\frac{\sin^2\theta}{8s}\lambda(s,m_N^2,m_\pi^2)\lambda(s,m_N^2,m_\omega^2)\right)\right],
\end{aligned} \tag{14}$$

where

$$q_\omega^2 = \frac{\lambda(t,m_\omega^2,m_\pi^2)}{4m_\omega^2}, \tag{15}$$

s is the squared invariant collision energy, t is the transferred four-momentum, θ is the emission angle, and $\lambda(x,y,z)$ is the triangular function. For the $\omega\rho\pi$ vertex a form factor is proposed [62],

$$F(t) = \frac{\Lambda^2 - m_\rho^2}{\Lambda^2 - t}, \tag{16}$$

while for the ρNN vertex

$$F(t,s) = \exp(\beta t)\exp(-\alpha s). \tag{17}$$

The parameters α, β, and Λ were extracted by fitting experimental data [62]. Their values are

$$\begin{aligned}
&\Lambda = 2.7\ \text{GeV}, \quad \beta = 2.3\ \text{GeV}^{-2},\\
&\alpha = 0.16\ \text{GeV}^{-2}.
\end{aligned} \tag{18}$$

(ii) For $\omega N \to \rho N$,

$$\frac{d\sigma}{dt} = -g_{\pi NN}^2 \frac{g_{\omega\rho\pi}^2}{m_\omega^2} t \frac{\left(t - m_\omega^2 - m_\rho^2\right)^2 - 4m_\omega^2 m_\rho^2}{96\pi\lambda\left(s, m_\omega^2, m_N^2\right)} \times \frac{F_{\omega\rho\pi}^2(t) F_{\pi NN}^2(t)}{\left(t - m_\pi^2\right)^2}, \quad (19)$$

where $g_{\pi NN} = 13.59$.

(iii) For $\omega N \to \pi\pi N$,

$$\sigma = \frac{1}{32\pi^2\lambda\left(s, m_\omega^2, m_N^2\right)} \int_{(m_N+m_\pi)^2}^{(\sqrt{s}-m_\pi)^2} ds_1 \lambda^{1/2}\left(s_1, m_\rho^2, m_N^2\right) \times \sigma_{\rho N\to\pi N}(s_1) \int_{t_-}^{t_+} dt \frac{g_{\omega\rho\pi}^2 F_{\omega\rho\pi}^2}{m_\omega^2\left(t - m_\rho^2\right)^2} \times \left[\left(t + m_\omega^2 - m_\pi^2\right)^2 - 4m_\omega^2 t\right], \quad (20)$$

where $\sigma_{\rho N\to\pi N}$ is the total cross section of $\rho N \to \pi N$ defined from the inverse reaction by using the detailed balance principle. This cross section was calculated using the resonance model as we describe below.

(iv) For elastic $\omega N \to \omega N$, the process is described by the σ-exchange model [62]. The model proposes the interaction Lagrangians

$$\mathcal{L}_{\sigma NN} = g_{\sigma NN} \bar{N} N \cdot \sigma, \quad (21)$$

$$\mathcal{L}_{\omega\sigma\omega} = g_{\omega\sigma\omega}(\partial^\alpha \omega^\beta \partial_\alpha \omega_\beta - \partial^\alpha \omega^\beta \partial_\beta \omega_\alpha)\sigma, \quad (22)$$

with the scalar coupling constants $g_{\sigma NN} = 10.54$, $g_{\omega\sigma\omega} = 1.76$ and monopole form factor $\Lambda = 2$ GeV at the σNN vertex. The differential cross section can be calculated as [62]:

$$\frac{d\sigma}{dt} = \frac{g_{\sigma NN}^2 g_{\omega\sigma\omega}^2}{16\pi m_\omega^2 \lambda\left(s, m_\omega^2, m_N^2\right)}(4m^2 - t) \times \frac{F_{\omega\sigma\omega}^2 F_{\sigma NN}^2}{\left(t - m_\sigma^2\right)^2}\left(m_\sigma^4 - \frac{m_\omega^2}{3} + \frac{t^2}{12}\right). \quad (23)$$

2. One-meson exchange model for J/Ψ meson

We also include the J/Ψ dissociations in the interaction with nucleons. The dissociation occurs through the nuclear reactions $J/\Psi N \to \Lambda_c \bar{D}$, $\to \Lambda_c \bar{D}^*$, and $\to N D \bar{D}$. To include them in the CRISP code we use the hadronic one-boson exchange model (EM) proposed by Sibirtsev, Tsushima, and Thomas [68]. The basic ideas of the model are sustained by the measurements reported by the NA50 Collaboration in the study of J/Ψ suppression in Pb + Pb collisions at the CERN Super Proton Synchrotron [69]. The model shows good agreement with the QCD first-order calculation at high invariant energies, but substantially deviates from it near the threshold.

The dissociation processes are shown in diagrams (a)–(d) of Fig. 2. According to the approach of Sibirtsev *et al.*, within the boson-exchange model, the interaction Lagrangian densities are [68]

$$\mathcal{L}_{JDD} = i g_{JDD} J^\mu [\bar{D}(\partial_\mu D) - (\partial_\mu \bar{D}) D], \quad (24)$$

$$\mathcal{L}_{DN\Lambda_c} = i g_{DN\Lambda_c} [\bar{N}\gamma_5 \Lambda_c D + \bar{D}\bar{\Lambda}_c \gamma_5 N], \quad (25)$$

$$\mathcal{L}_{JD^*D} = \frac{g_{JD^*D}}{m_J} \varepsilon_{\alpha\beta\mu\nu}(\partial^\alpha J^\beta)[(\partial^\mu \bar{D}^{*\nu}) D + \bar{D}(\partial^\mu D^{*\nu})], \quad (26)$$

$$\mathcal{L}_{D^*N\Lambda_c} = -g_{D^*N\Lambda_c}[\bar{N}\gamma_\mu \Lambda_c D^{*\mu} + \bar{D}^{*\mu}\bar{\Lambda}_c \gamma_\mu N], \quad (27)$$

with

$$N = \begin{pmatrix} p \\ n \end{pmatrix}, \quad \bar{N} = N^\dagger \gamma_0, \quad D \equiv \begin{pmatrix} D^0 \\ D^+ \end{pmatrix}, \quad \bar{D} = D^\dagger. \quad (28)$$

For D^* and $\bar{D}^*$ a similar notation is used. The interaction vertices are characterized by coupling constants $g_{JDD} = g_{JDD^*} = 7.64$, $g_{DN\Lambda_c} = 14.8$, $g_{D^*N\Lambda_c} = -19$, and an associated form factor parametrized in a conventional monopole form:

$$F(t) = \frac{\Lambda^2}{\Lambda^2 - t}. \quad (29)$$

Λ is the cutoff parameter explicitly defined by $\Lambda = 3.1$ for JDD and JDD^* vertices while $\Lambda = 2$ for $DN\Lambda_c$ and $D^*N\Lambda_c$ vertices.

The differential cross sections for the nucleon and J/Ψ meson interactions for the processes represented in diagrams (a)–(c) of Fig. 2 are given by [68]

$$\frac{d\sigma_{a,b}}{d\Omega} = \frac{1}{64\pi^2 s}\overline{|M_{a,b}|}^2 \times \left(\frac{[(m_\Lambda + m_D)^2 - s][(m_\Lambda - m_D)^2 - s]}{[(m_N + m_{J/\Psi})^2 - s][(m_N - m_{J/\Psi})^2 - s]}\right)^{1/2} \quad (30)$$

$$\frac{d\sigma_c}{d\Omega} = \frac{1}{64\pi^2 s}\overline{|M_c|}^2 \times \left(\frac{[(m_\Lambda + m_{D^*})^2 - s][(m_\Lambda - m_{D^*})^2 - s]}{[(m_N + m_{J/\Psi})^2 - s][(m_N - m_{J/\Psi})^2 - s]}\right)^{1/2}, \quad (31)$$

with s being the squared invariant collision energy, and the $\overline{|M_{a,b,c}|}^2$ terms are the corresponding squared amplitudes, averaged over the initial spins and summed over the final spins. The squared amplitudes of the processes are given by [68]

$$\overline{|M_a|}^2 = \frac{8 g_{JDD}^2 g_{DN\Lambda_c}^2}{3m_{J/\Psi}^2}\left(\frac{1}{q^2 - m_D^2} + \frac{1}{2p_{J/\Psi}\cdot p_{\bar{D}}}\right)^2 \times (p_N \cdot p_{\Lambda_c} - m_N m_{\Lambda_c})\left[(p_{J/\Psi}\cdot p_{\bar{D}})^2 - m_{J/\Psi}^2 m_{\bar{D}}^2\right], \quad (32)$$

$$\overline{|M_b|}^2 = \frac{g_{JD^*D}^2 g_{D^*N\Lambda_c}^2}{3m_{J/\Psi}^2}\frac{1}{\left(q^2 - m_{D^*}^2\right)^2} \times \left\{m_{J/\Psi}^2\left[p^2 q^2 - \left(m_{\Lambda_c}^2 - m_N^2\right)^2\right] + 2(p_{J/\Psi}\cdot p) \times (p_{J/\Psi}\cdot q)\left(m_{\Lambda_c}^2 - m_N^2\right) - p^2(p_{J/\Psi}\cdot q)^2 - q^2(p_{J/\Psi}\cdot p)^2 - 4\left(p_N\cdot p_{\Lambda_c} - m_N m_{\Lambda_c}\right)\left[m_{J/\Psi}^2 q^2 - (p_{J/\Psi}\cdot p)^2\right]\right\} \quad (33)$$

$$\overline{|M_c|}^2 = \frac{4g_{JD^*D}^2 g_{DN\Lambda_c}^2}{3m_{J/\Psi}^2} \frac{1}{\left(q^2 - m_D^2\right)^2} \left(p_N \cdot p_{\Lambda_c} - m_N m_{\Lambda_c}\right) \times \left[\left(p_{J/\Psi} \cdot p_{\bar{D}^*}\right)^2 - m_{J/\Psi}^2 m_{\bar{D}^*}^2\right], \quad (34)$$

where $q \equiv p_{J/\Psi} - p_{\bar{D}} = p_{\Lambda_c} - p_N$ denotes the transferred four-momentum and $p \equiv p_{\Lambda_c} + p_N$.

The double differential cross section for the reaction $J/\Psi + N \to N + D + \bar{D}$ is shown in diagram (d) of Fig. 2 and can be written as [68]

$$\frac{d^2\sigma_d}{dt\,ds_1} = \frac{g_{J/\Psi DD}^2}{96\pi^2 q_{J/\Psi}^2 s} q_D \sqrt{s_1} \frac{F^2(t)}{\left(t - m_D^2\right)^2} \times \frac{[(m_{J/\Psi} + m_D)^2 - t][(m_{J/\Psi} - m_D)^2 - t]}{m_{J/\Psi}^2} \times \sigma_{DN}(s_1), \quad (35)$$

where

$$q_D^2 = \frac{[(m_N + m_D)^2 - s_1][(m_N - m_D)^2 - s_1]}{4s_1}, \quad (36)$$

$$q_{J/\Psi}^2 = \frac{[(m_N + m_{J/\Psi})^2 - s][(m_N - m_{J/\Psi})^2 - s]}{4s}. \quad (37)$$

The total DN and $\bar{D}N$ cross sections can be parametrized as [70]

$$\sigma_{\bar{D}N}(s_1) = \left(\frac{\left[\left(m_{\Lambda_c} + m_\pi\right)^2 - s_1\right]\left[\left(m_{\Lambda_c} - m_\pi\right)^2 - s_1\right]}{[(m_N + m_D)^2 - s_1][(m_N - m_D)^2 - s_1]}\right)^{1/2} \times \frac{27}{s_1} + 20, \quad (38)$$

with m_{Λ_c} and m_π being the hyperon and pion masses respectively, given in GeV, and the cross section being given in millibarns.

3. Resonance model: ρ, ω, and ϕ mesons

For the inclusion of $\pi N \to \rho N$, $\to \omega N$, and $\to \phi N$ interaction channels we included the best-fit results using the resonance model (RM) carried out by Sibirtsev, Cassing, and Mosel [71]. The collisions included in CRISP by this model are shown in Fig. 3. In this work the cross section for the ρ, ω, and ϕ vector meson production from the pion-induced nuclear reaction is given by means of the reaction

$$\pi + N \to R \to M + N, \quad (39)$$

where R is a barionic resonance. Assuming that the squared matrix element is proportional to the Breit-Wigner function, the cross section can be proposed as

$$\sigma_{\pi+N\to M+N}(s) = \frac{\pi}{k^2} \frac{2J+1}{2} \frac{B_{\text{in}} B_{\text{out}} \Gamma^2}{(\sqrt{s} - M_R)^2 + \Gamma^2/4} \times R_2(s), \quad (40)$$

where J is the resonance spin and B_{in}, B_{out} are the width of the incident and scattered particles respectively. The momentum phase space volume of the final particles is given by $R_2(s) = \pi\lambda(s,m_M^2,m_N^2)/\sqrt{s}$. The k^2 term represent the triangular function $k^2 = \lambda(s,m_\pi^2,m_N^2)$ while parameters M_R and Γ are the mass and the width of the resonance.

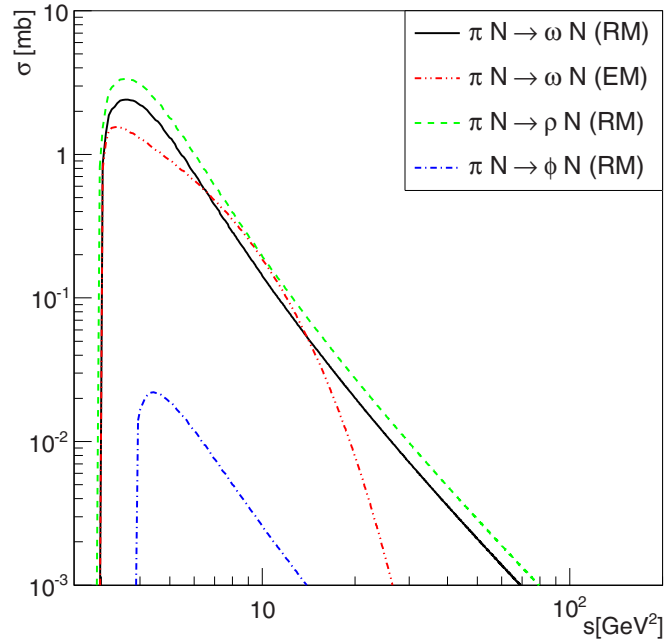

FIG. 5. (Color online) The total cross sections of various channels for the nuclear reaction $\pi N \to VN$ included in the CRISP code using the one-meson exchange model (EM), the resonant model (RM), and the detailed balance principle.

The cross sections per interacting particle for all in-medium process included in CRISP are shown in Figs. 5 (π), 6 (ρ), 7 (ω),

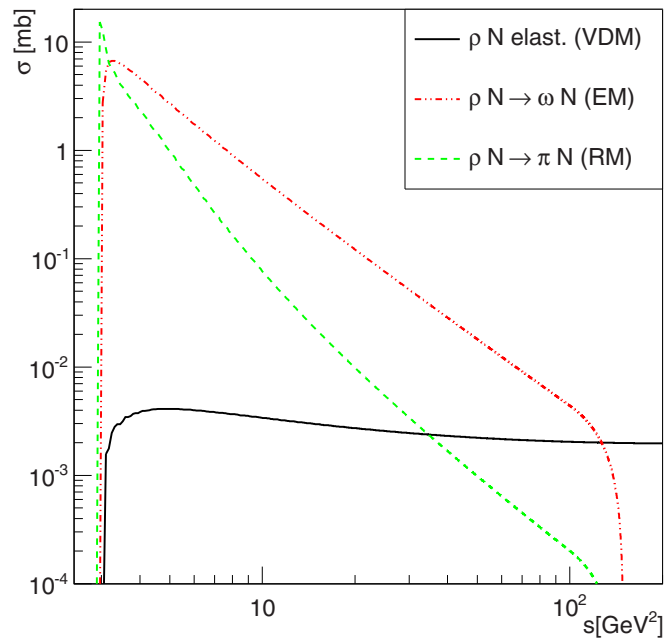

FIG. 6. (Color online) The total cross sections of various channels for the nuclear reaction $\rho N \to VN$ included in the CRISP code using the vector dominance model (VDM), the one-meson exchange model (EM), the resonant model (RM), and the detailed balance principle.

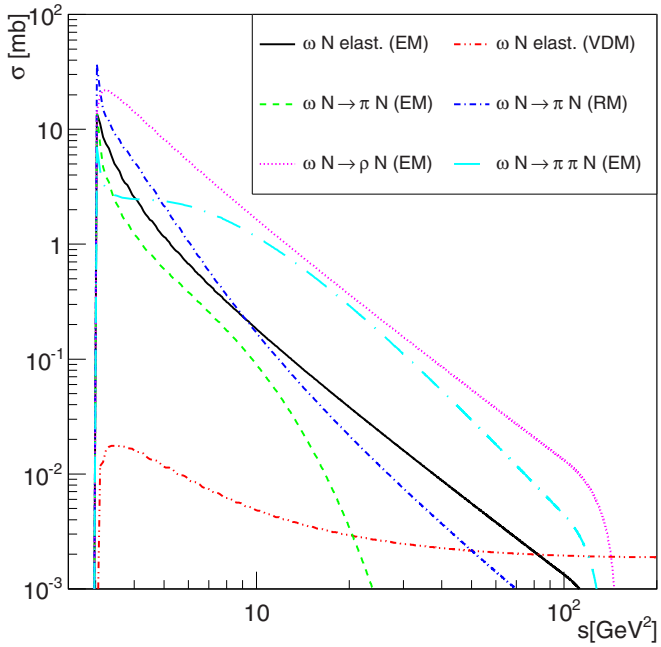

FIG. 7. (Color online) The total cross sections of various channels for the nuclear reaction $\omega N \to V N$ included in the CRISP code using the vector dominance model (VDM), the one-meson exchange model (EM), the resonant model (RM) and the detailed balance principle.

8 (ϕ), and 9 (J/Ψ) for the one-meson exchange model (EM), the resonant model (RM), and the vector dominance model (VDM). Both resonant and one-meson exchange models supply the $\omega N \to \pi N$ reaction cross section. We use the

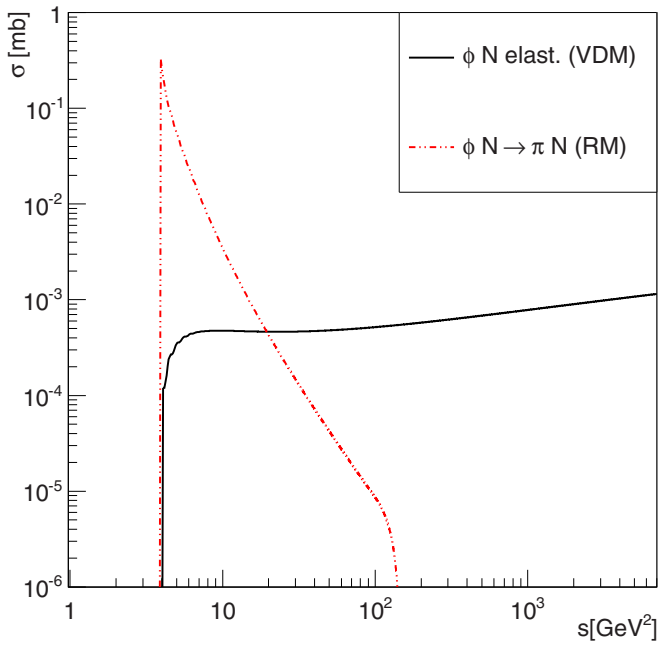

FIG. 8. (Color online) The total cross sections of various channels for the nuclear reaction $\phi N \to V N$ included in the CRISP code using the vector dominance model (VDM), the resonant model (RM) and the detailed balance principle.

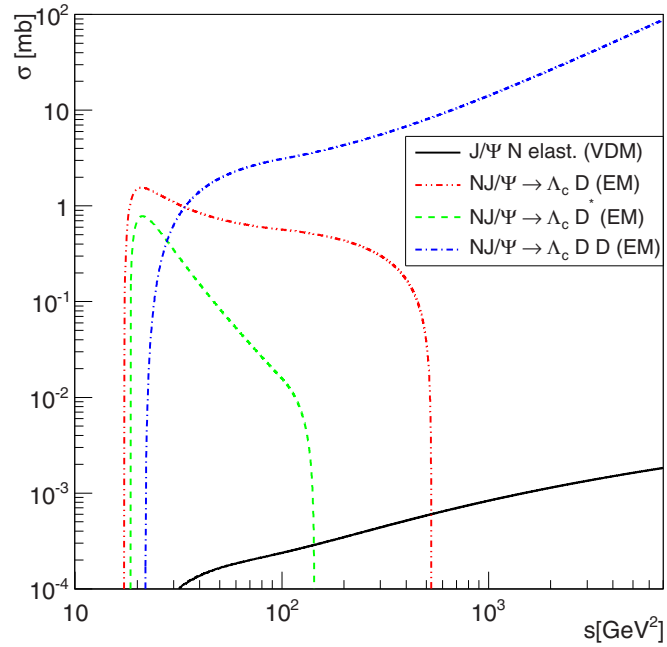

FIG. 9. (Color online) The total cross sections of various channels for the nuclear reaction $J/\Psi N \to V N$ included in the CRISP code using the vector dominance model (VDM) and the one-meson exchange model (EM).

resonant model, since it reproduces better the total cross section experimental data [71], as we show in Fig. 10. The elastic cross section $\omega N \to \omega N$ provided by the one-meson exchange model is chosen over the elastic cross section calculated using the vector dominance model since it can be only used at very high energies. We note the importance of

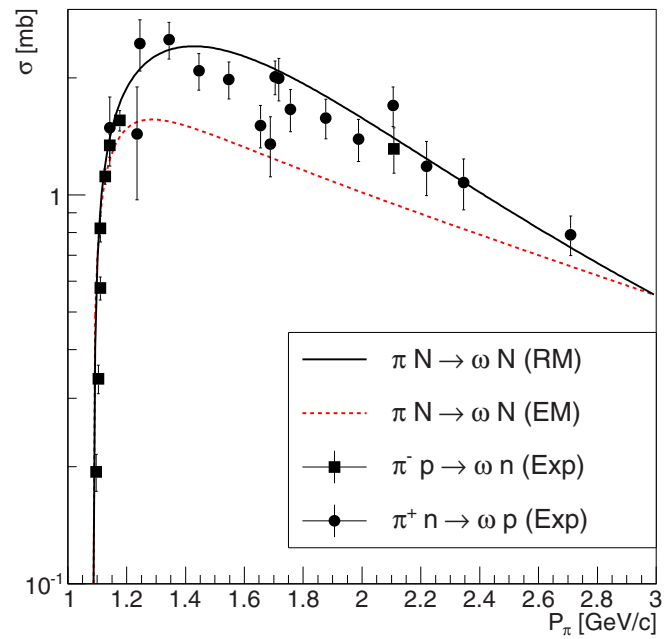

FIG. 10. (Color online) The comparison between the total cross sections of the nuclear reaction $\pi N \to \omega N$ given by the one-meson exchange model (EM) and the resonant model (RM).

these nuclear reactions above the vector meson production threshold, especially $\omega N \to \rho N$ and $\omega N \to \pi N$. At very high center-of-mass energies these reactions become less important in the FSI of these mesons. This behavior is different for J/Ψ interaction with nucleons, where total cross section increases with increasing center-of-mass energy.

III. RESULTS AND DISCUSSIONS

The mechanisms for vector meson photoproduction and FSI processes described above were incorporated in the intranuclear cascade phase in the CRISP code. We proceed to describe the photonuclear production of those mesons and study how the nuclear medium modifies the relevant observables in those reactions.

First we simulated photoproduction of vector mesons ρ, ω, and ϕ for nuclei at a fixed energy value ($E_\gamma = 9$ GeV) looking for the effective mass index A_{eff} which carries the nucleus effect of this process. In a second simulation, we simulate the nuclear photoproduction process for a single nucleus, ^{12}C, at several energies with a higher statistics level and calculated the bound nucleon cross section using the previously archived effective mass index. We obtain A_{eff} for vector meson J/Ψ using a different method, since it has a very low cross section value at $E_\gamma = 9$ GeV. After that we calculate the subthreshold photoproduction for the J/Ψ meson. In this simulation we use a high statistics level and model the photoproduction process for nuclei at a several energies near threshold, so we can evaluate the $A_{\text{eff}}(E_\gamma)$ behavior that permits us to obtain the effective mass index for J/Ψ used in the second step. Also an exponential behavior related to a blocking mechanism and shadowing effect was obtained in this study. The Pauli blocking effect on the vector meson mass generation in CRISP code was also analyzed in these simulations. In order to study the final state interaction (FSI) of vector mesons, we studied a J/Ψ -A compound nucleus with and without FSI, and the ω meson nuclear transparency. In the following, we present some of the results obtained compared with experimental data. We discuss the results and emphasize the nuclear effects on the production of mesons.

A. Photoproduction of mesons ρ, ω, and ϕ: Cross section versus atomic number

Photoproduction of ρ, ω, and ϕ mesons was simulated with CRISP code at 9 GeV on nuclei ^{12}C, ^{27}Al, ^{40}Ca, ^{56}Fe, ^{63}Cu, ^{107}Ag, ^{138}Ba, ^{153}Eu, ^{166}Er, ^{180}W, ^{197}Au, ^{208}Pb, and ^{232}Th. We observe a good agreement between calculations and experimental data; both show a clear deviation from the linear behavior. The resulting ρ_0, ω, and ϕ yields obtained for each meson are $\sim 10^4$, $\sim 10^3$ and $\sim 3 \times 10^2$ with a statistical error of $\sim$1%, $\sim$3% and $\sim$6% respectively. In Fig. 11 we present the calculated cross section for each meson studied, normalized by the corresponding proton cross section. For comparison we include experimental data from Ref. [72] and the dotted line indicating a linear increase of the cross section with the nuclear mass number.

Due to the strong interaction of the hadronic component of the photo wavefunction, the photon does not see the entire nuclei. Indeed, part of the nucleons fall in the shadowing region, therefore the cross section is not proportional to the mass index A (linear dependence), but to an effective mass index A^α. This is a well known consequence of the vector meson dominance in photonuclear interactions. The exponent α is determined by fitting the function

$$\sigma_{VA}(A) = \sigma_0 A^\alpha, \tag{41}$$

to the results obtained with the CRISP code. Here σ_0 and α are free parameters, whose best fits are obtained with values presented in Table I, for each studied vector meson. We observed that the exponent α is very similar for all mesons. This can be understood in view of the energy of the analyzed reaction, 9 GeV. This energy is far above the threshold for any meson, so that the shadowing effect is already saturated [73]. Therefore we performed a single fit for all CRISP data shown by the red line in the Fig. 11, which represents an average over all mesons. The exponent α resulting from this comprehensive fitting is $\alpha = 0.87 \pm 0.01$.

The parameter σ_0 in Eq. (41) is usually considered as the bound-nucleon cross section. In Table I, this value is compared

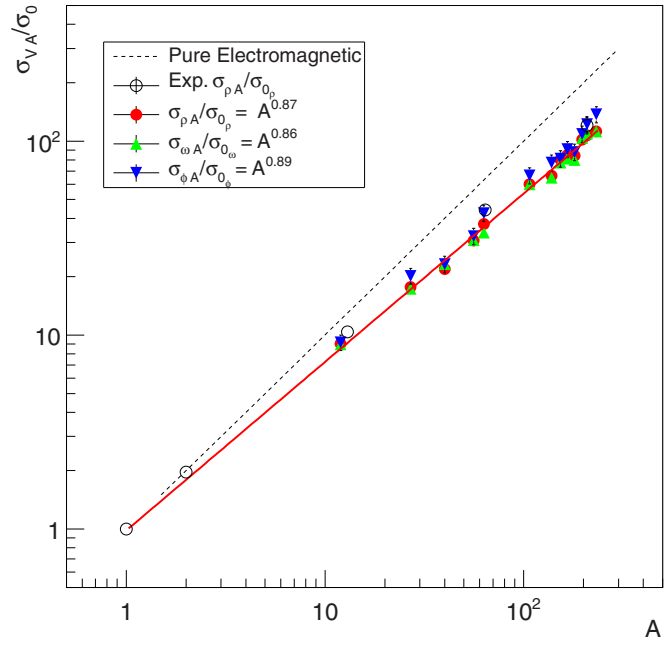

FIG. 11. (Color online) The ratio of vector meson photoproduction cross section for several A nuclei to the obtained binding nucleon cross section (σ_0) at $E_\gamma = 9$ GeV with the CRISP code. Figure also shows the all-meson general fit using Eq. (41) in comparison with ρ experimental data. The parameters for the best fit are $\sigma_0 = 0.98 \pm 0.03$ and $\alpha = 0.87 \pm 0.01$ with $\chi^2_{\text{red}} = 3.5$.

TABLE I. Results of the CRISP data fitted to $\sigma_{VA} = \sigma_0 A^\alpha$ at 9 GeV.

Meson	σ_0 (mb)	α	$\sigma_{0_{\text{theo}}}$ (mb)	$\sigma_{0_{\text{exp}}}$ (mb)
ρ^0	16.8 ± 0.3	0.87 ± 0.01	12.6	$\sim 10.4 \pm 0.7$
ω	2.06 ± 0.10	0.88 ± 0.01	1.55	$\sim 1.10 \pm 0.18$
ϕ	0.58 ± 0.05	0.90 ± 0.02	0.46	$\sim 0.55 \pm 0.09$

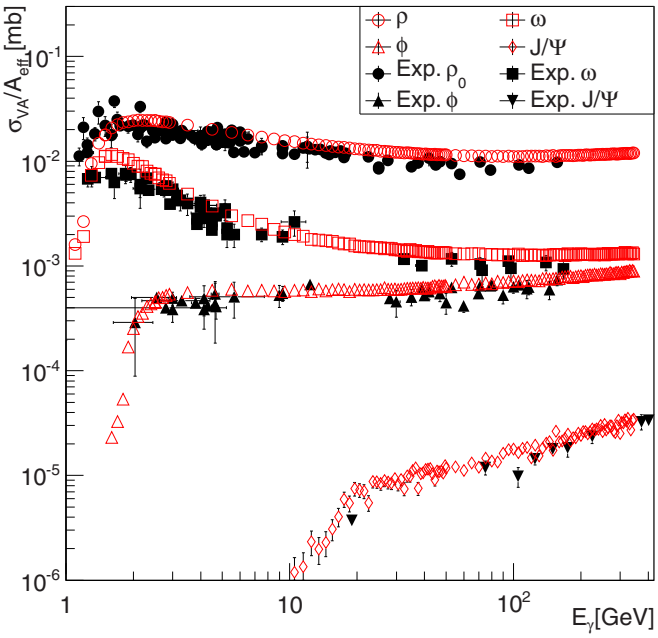

FIG. 12. (Color online) Total cross sections for vector meson photoproduction on nucleons obtained with the CRISP code in comparison with experimental data.

to the proton cross section, where it can be observed that our result surpasses both theoretical and experimental cross section values at that energy; however, values are similar. For the ϕ meson the result is according to experimental data that is smaller for all mesons than the predictions of the soft Pomeron model. It is important to note that the bound-nucleon cross section reflects contributions from protons and neutrons inside the nucleus.

The shadowing effect observed in our calculations is a pure nuclear effect which depends on the photoproduction cross section and on nuclear properties such as density and radius. The fact that a good description of this effect is obtained is evidence that the photon propagation in the nucleus and its interaction with the nucleons are correctly taken into account in the present calculations.

The factor A^{α} in Eq. (41) is the effective number of nucleons participating in the absorption of the photons, while σ_0 is the bound-nucleon cross section. Since protons and neutrons present similar cross sections in the photon energy range considered in the present work, the bound-nucleon cross section should be similar to the proton's.

In Fig. 12 we compared the resulting bound-nucleon cross section for vector meson photoproduction. In this calculation we use the exponent values obtained from the previous fit for ρ, ω, and ϕ mesons, as shown in Table I. For meson J/Ψ we use $\alpha = 0.94$ since this value corresponds to the saturated shadowing effect that we calculated below. We observed an overall good agreement between calculation and experiment over the entire range from the respective vector meson threshold up to a few hundreds of GeV in the laboratory frame of reference. Some deviation between calculation and data can be observed near the threshold, but it may be attributed to the use of constant α, while it is known that near threshold some dependence on photon energy should be expected. This effect will be studied in more detail below for the case of J/Ψ photoproduction.

B. Subthreshold photoproduction of vector mesons

Important information on the nuclear medium can be gathered from the photoabsorption process near threshold, since the amplitude of the reaction is modified by nuclear constraints such as conservation laws and Pauli blocking effects. Such constraints remarkably take place at low kinetic energy values of the particles resulting from the reaction. The photoproduction near the threshold of vector mesons is very useful to study processes that strongly depends on such constraints, e.g., the final state interaction for particles and the existence of bound states for heavier particles such as ϕ and J/Ψ mesons. Near this energy, the particles will remain on nuclei a longer time before they can go out. This blocking mechanism has strong effects on cross section, but is suppressed by another mechanism: the Fermi motion of nucleons. The Fermi motion modifies the energy of the photon-nucleon system and it has strong influence when the kinetic energy of the particles involved in a process is of the same order as the Fermi kinetic energy of the nuclei. We will discuss next how both effects modify subthreshold photoproduction.

1. *Shadowing effect near the threshold*

As already stated, the shadowing effect shows an energy dependence near the vector meson threshold expressed by the α exponent in Eq. (41), which cannot be considered constant. The effects of the nuclear medium on vector meson photoproduction manifest more strongly near threshold, where the secondary nucleon has low energy and therefore the Pauli blocking mechanism is more effective. In order to evaluate the importance of this mechanism we define the Pauli blocking index:

$$\eta = \frac{\eta_b}{\eta_c} \tag{42}$$

where η_b is the number of vector mesons that have their photoproduction blocked because of Pauli principle observation, and η_c is the number of vector mesons effectively created. The Pauli blocking index is fitted to an exponential function,

$$\eta = \alpha e^{\beta E_\gamma} \tag{43}$$

In Fig. 13 we report the fit obtained for the Pauli blocking index in J/Ψ photoproduction on the ^{238}U nucleus at energies around threshold. As the photon energy decreases, the index η increases from $\sim$0 at $E_\gamma = 11.5$ GeV to $\sim$7 at $E_\gamma = 7.5$ GeV. Observe that this effect is more intense below the J/Ψ threshold energy on photons. This calculation should give an idea of how an effective mass index must behave since the Pauli blocking mechanism is the main nuclear effect that modifies photoproduction processes near threshold.

The photoproduction section for J/Ψ was calculated on nuclei ^{40}Ca, ^{63}Cu ^{107}Ag, ^{138}Ba, ^{166}Er, ^{180}W, ^{208}Pb, and ^{238}U at several energies in the range $7 \leqslant E_\gamma \leqslant 14$ GeV. The result at each energy for all nuclei studied here was fitted to Eq. (41)

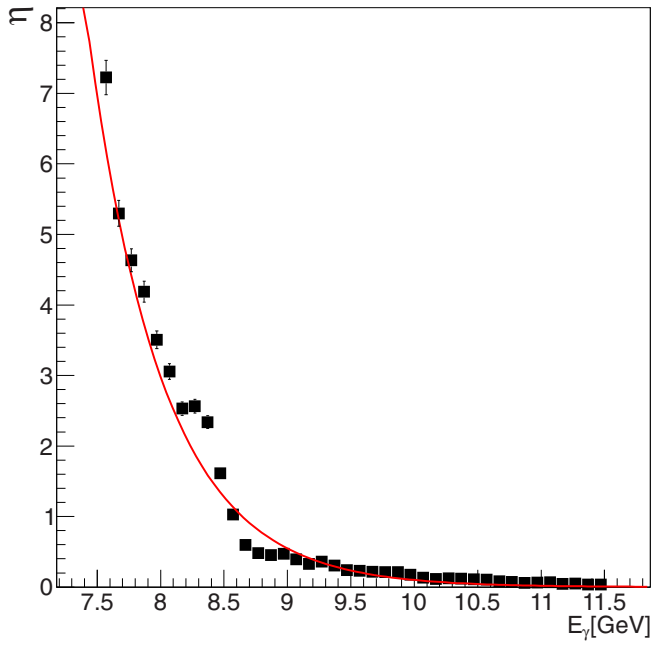

FIG. 13. (Color online) Pauli blocking index fit (red line) on photoproduction of J/Ψ mesons near the threshold. The parameters for the best fit are $\alpha = 2.3 \times 10^6 \pm 3.5 \times 10^5$ and $\beta = -1.7 \pm 0.02$ with $\chi^2_{\text{red}} = 5.5$.

with σ_0 and α used as free parameters. The α values obtained for each energy are plotted in Fig. 14, where it can be noted that α increases as photon energy decreases.

To describe quantitatively the behavior with the energy we fit the calculated data to the function

$$\alpha(E_\gamma) = \alpha_0 + e^{\beta(E_\gamma - E_0)}, \tag{44}$$

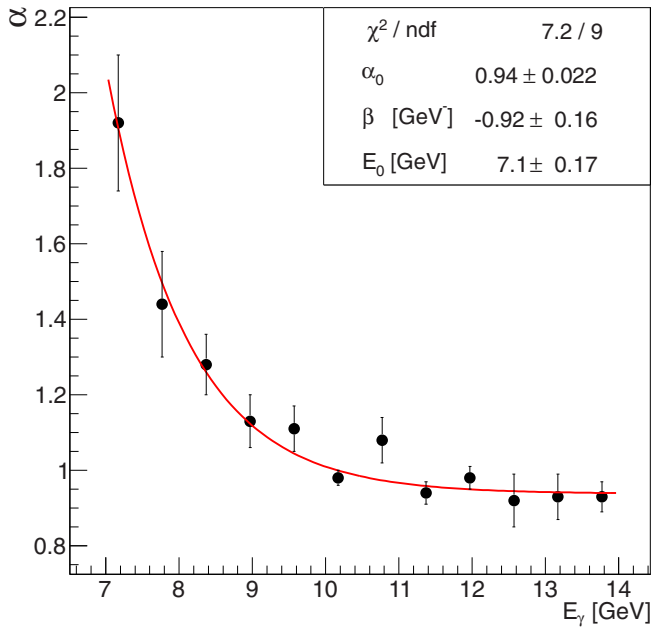

FIG. 14. (Color online) α exponent fit (red line) on J/Ψ meson photoproduction near threshold.

obtaining a good description of the result. It is important to emphasize two things: first, that two different mechanisms combine themselves to produce the observed behavior of $\alpha(E_\gamma)$–namely, the Pauli blocking and the shadowing effects—and second, that we obtain an exponential $\alpha(E_\gamma)$ behavior, similar to that previously obtained in the Pauli blocking index calculation. The obtained parameter $\alpha_0 = 0.94$ at $\alpha(E_\gamma)$ energies far from threshold corresponds to the saturated shadowing effect, used in the photon cross section calculation for a bound nucleus. At these energies Pauli blocking is almost missed, as we can check with the Pauli blocking index calculation. The parameter $E_0 = 7.1$ GeV can be considered as the new threshold energy in the laboratory frame. This new threshold is now set by the Pauli mechanism. Below this photon energy value, photoproduction can actually occur, according to Fermi motion of nucleons, but the Pauli blocking mechanism is so intense that it blocks any photoproduction process. The behavior of $\alpha(E_\gamma)$ permits us to obtain the correct bound-nucleon cross section near the threshold. Below we describe how it is calculated.

2. *Subthreshold photoproduction of J/Ψ on ^{238}U nucleus*

We are now able to calculate the photoproduction cross section near threshold with a revised effective mass index which takes into account the threshold constraints and the Fermi motion in a more realistic way. All these constraints are resumed on the new mass index, whose exponent is substituted by Eq. (44),

$$A^\alpha \rightarrow A^{\alpha(E_\gamma)}. \tag{45}$$

The function $\alpha(E_\gamma)$ is an effective exponent representing several effects that modify the photoabsorption cross section, so we do not attribute any physical meaning to this parameter. In Fig. 15 we present the results from our study of J/Ψ subthreshold photoproduction on the ^{238}U nucleus. For comparison we show also the cross section for J/Ψ photoproduction on protons, where the threshold can be clearly seen at $E_\gamma \sim 8.2$ GeV. The results obtained are shown with two different normalizations. In one case (red squares) the bound nucleon cross section is obtained through Eq. (41) with the saturated exponent $\alpha = 0.94$. In the second case (black dots) the bound nucleon cross section is obtained considering it to be dependent on the photon energy, since near the threshold the shadowing effect has not saturated yet.

In both results for bound nucleons we can observe a significant J/Ψ production below the energy threshold for its photoproduction on protons. As discussed above, this is an expected consequence of Fermi motion. In fact, due to the nucleon motion inside the nucleus, the component of its momentum in the direction of the incident photon momentum can vary by $\Delta p \equiv 48$ MeV, which corresponds to a variation of the γ-N system energy in the center-of-mass frame of $\Delta W \equiv 570$ MeV. In the laboratory frame of reference it corresponds to $\Delta E_\gamma \equiv 5.4$ GeV.

The photon energy fluctuation is thus $\Delta E_\gamma/2 = 2.7$ GeV below or above threshold, and it has clear consequences on the cross section. In fact the black dotted results show not only

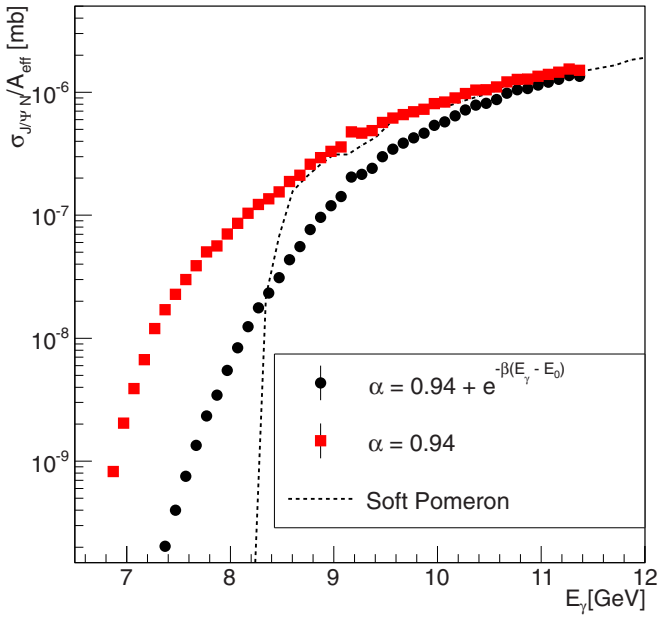

FIG. 15. (Color online) Total cross sections per nucleon for J/Ψ meson photoproduction near threshold using different normalizations: with saturated shadowing effect (red squares) and with energy-dependence shadowing effect (black circles).

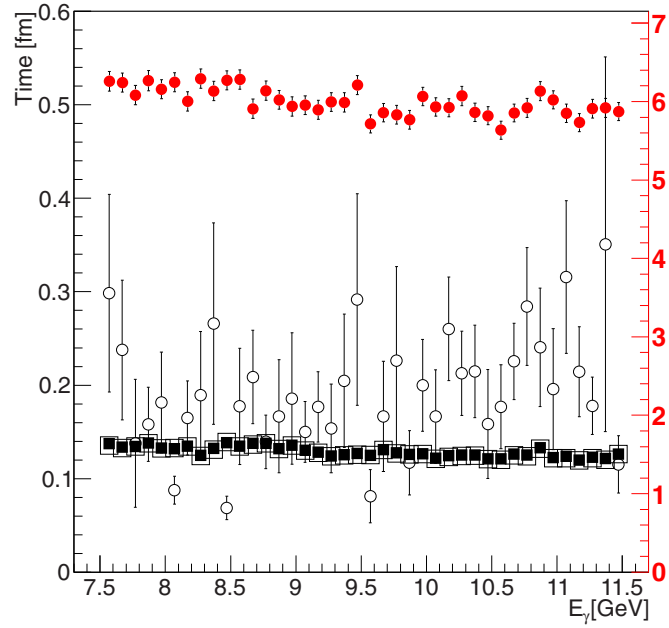

FIG. 16. (Color online) Bound J/Ψ half-life time near the threshold with (black squares) and without (red filled circles) FSI. Half-life time with FSI includes two dissociation processes: by emission from the nucleus (open circles) and by interaction with nucleons (open squares). The right-hand y axis stands for half-life time without FSI.

a subthreshold production of J/Ψ, but also a cross section which increases more smoothly than for protons, due to the Fermi motion of the nucleons

C. Bound J/Ψ half-life

With the CRISP code we can study dynamical effects on the width of the compound system formed by the meson and the nucleus. This is an aspect of vector meson photoproduction which has deserved increasing attention due to the possibility of investigation of QCD color van der Waals forces [74] in nuclei. Also a possible negative mass shift on the meson can result from its binding to the nucleus. However, also here the pure nuclear effect is present and it must be correctly taken into account before studying QCD effects.

The half-life of J/Ψ in ^{238}U was studied, and the results are shown in Fig. 16. Here we reported the calculated half-life for the bound J/Ψ (black squares), which includes two decay mechanisms, namely, J/Ψ dissociation due interactions with nucleons and the J/Ψ emission from the nucleus, which we call the unbinding process. We can analyze separately both processes and report the half-life due to unbinding as open circles and the dissociation time as open squares. In addition, the unbinding process is studied without the FSI (red filled circles).

The dissociation times with FSI, which are around 0.14 fm (open squares), are practically identical to the bound J/Ψ half-life with FSI (black squares). This result indicates that the main decay mechanism is dissociation, so just a small fraction of the J/Ψ will escape from the nucleus. We also studied the unbinding half-life with FSI (open circles), which is around 0.18–0.25 fm. This unbinding process corresponds to those J/Ψ which are produced near the nuclear surface and can escape before interacting with any nucleon inside the nucleus. In fact the unbinding half-life obtained by switching off all FSIs (red filled circles) is around 6 fm, close to the nuclear radius, so the open circles indeed represent J/Ψ near surface.

D. The ρ mass spectra

The mass spectrum for the ρ meson, $A(\mu)$, has been obtained by calculating the cross section for ρ-meson production including the leptonic decay width [75]:

$$A(\mu) = \frac{2}{\pi} \frac{\mu^2 \Gamma(\mu)}{\left(\mu^2 - m_\rho^2\right)^2 + \mu^2 \Gamma^2(\mu)}, \tag{46}$$

where $\Gamma(\mu)$ is the width of the resonance, m_ρ is the ρ pole mass, and μ is the e^+e^- invariant mass. Equation (46) can be substituted with good approximation by the Breit-Wigner function divided by the factor μ^3.

The CRISP code generates the hadron mass by the random selection of a Breit-Wigner function according to its lower and upper limits defined by the hadron width. In order to guarantee energy conservation the condition $m_V < \sqrt{s} - m_N$ must be satisfied. Here m_V is the meson mass and m_N is the nucleon mass. The hadron mass generation is also modified by Fermi motion and Pauli blocking.

In Fig. 17 is shown the mass distribution generated by the photoproduction process for photons with energy $E_\gamma =$ 1.1 GeV on nucleus ^{56}Fe compared with experimental data [76]. We observe that the ρ mass spectrum is not symmetric, showing a slower increase of the yield as the mass increases up to $\sim m_\rho$ and a sharp decrease of the yield above this mass. This

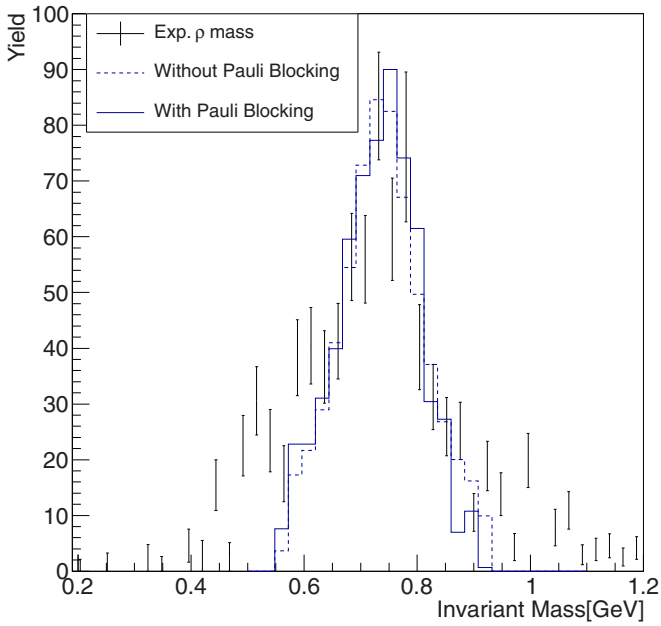

FIG. 17. (Color online) The ρ mass spectrum for the photoproduction on ^{56}Fe compared with experimental data [76].

sharp decrease is partially due to the Pauli blocking mechanism of the final state nucleon. In fact, the higher is the meson effective mass the lower is the momentum of the nucleon and therefore the stronger is the blocking effect. The effectiveness of Pauli blocking can be observed by comparing the full line in Fig. 17, which corresponds to the results obtained including the Pauli blocking mechanism, with the dashed line, corresponding to the calculations without the Pauli blocking. In the second case the peak is approximately symmetric, with a slow decrease of the yield as the mass increases above the peak value.

E. Nuclear transparency for the ω meson

We can observe in Figs. 6 and 7 that ρ and ω mesons present the highest cross sections with the nucleon in the FSI. For this reason the nuclear medium is less transparent to those mesons than to others. The transparency is defined as

$$T = \frac{\sigma_{\gamma A \to VX}}{A\sigma_{\gamma N \to VX}}, \tag{47}$$

meaning, the ratio of the inclusive nuclear photoproduction cross section is divided by A times the same quantity for the nucleon. T describes the loss of particle flux in nuclei which is related to the absorptive part of the nuclear potential of the particle. In order to avoid systematic uncertainties and to eliminate the nucleon cross section, the transparency ratio is usually normalized to carbon data, i.e.,

$$T = \frac{12\sigma_{\gamma A \to VX}}{A\sigma_{\gamma^{12}C \to VX}}. \tag{48}$$

While the ρ meson has a short half-life, decaying inside the nucleus, the ω meson can last long enough to propagate through the nuclear medium and escape, so this meson is one of the best candidates to study the nuclear transparency. In fact this was already done experimentally in Refs. [77–82].

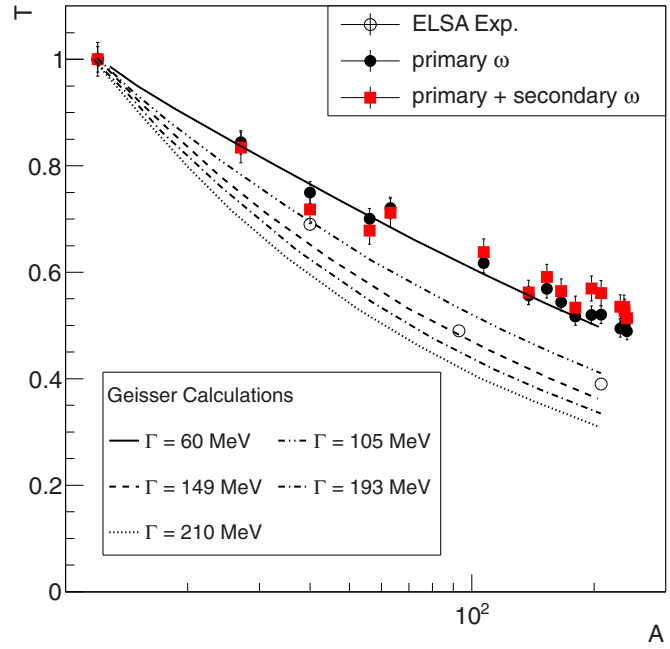

FIG. 18. (Color online) Normalized transparency ratio for the ω meson obtained with CRISP code according to Eq. (48) at $E_\gamma = 1.7$ GeV in comparison with theoretical Monte Carlo simulation, varying the width [77].

In Figs. 18 and 19 we present the calculation of the transparency for the ω photoproduction process at several mass indexes A. We illustrate two different results: the first includes all ω productions (red squares) while the second takes only into

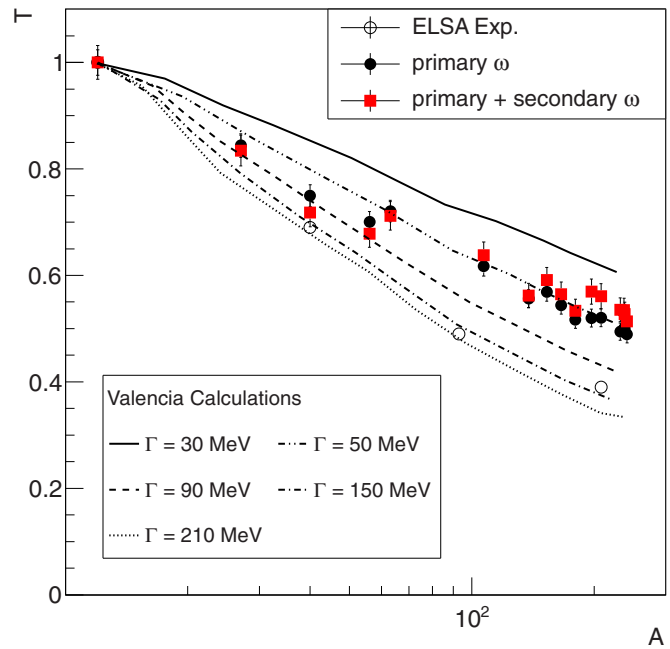

FIG. 19. (Color online) Normalized transparency ratio for the ω meson obtained with CRISP code according Eq. (48) at $E_\gamma = 1.7$ GeV in comparison with theoretical BUU calculation, varying the width [77].

account the primary ω production (black circles). We compare them to experimental data [77] and with calculations according two different models, namely, the Boltzmann-Uehling-Uhlenbeck transport code calculation by the Geissen group [77] and a Monte Carlo analysis by the Valencia group [77]. Experimental data were obtained in the Crystal Barrel/TAPS detector at the ELSA tagged photon facility in Bonn [77]. Our calculations are performed at photon energy $E_\gamma = 1.7$ GeV, which is the averaged energy of the experimental range.

We observe that the transparency calculated with the CRISP code deviates from experimental data and from the theoretical predictions. This is an indication that we are still missing some important channel in FSI. We are currently working to improve this aspect in our calculation.

IV. CONCLUSIONS

In this work we report the inclusion of vector meson photoproduction in the Monte Carlo code named CRISP. The photonucleon production was implemented according the soft dipole Pomeron model, developed by Martynov, Predazzi and Prokudin.

The final state interaction is taken into account by considering several channels of interaction of vector mesons with nucleons. We used three models: the one-boson exchange model proposed by Lykasov, Cassing, Sibirtsev, and Rzjanin, the one-boson exchange model proposed by Sibirtsev, Tsushima, and Thomas, and the resonance model carried out bySibirtsev, Cassing, and Mosel.

After presenting details of the vector meson photoproduction, we show that our calculations for protons are in good agreement with the experimental data. We studied several purely nuclear effects, such as Pauli blocking, Fermi motion, subthreshold photoproduction, and shadowing. Also, the half-life of J/Ψ in the nucleus was calculated, and was found to be much smaller than that of J/Ψ in the vacuum. This is due to the high cross section of J/Ψ with nucleons resulting in a fast dissociation of the meson.

ACKNOWLEDGMENTS

We acknowledge support from the Brasilian agency CNPQ under Grants No. 1141168/2010-2 (I.G.) and No. 305639/2010-2 (A.D.).

[1] V. Muccifora, N. Bianchi, A. Deppman, E. De Sanctis, M. Mirazita, E. Polli, P. Rossi, R. Burgwinkel, J. Hannappel, F. Klein, D. Menze, W. J. Schwille, and F. Wehnes, Phys. Rev. C **60**, 064616 (1999).

[2] M. Anghinolfi, V. Lucherini, P. Rossi, N. Bianchi, P. Corvisiero, A. Deppman, E. De Sanctis, A. Ebolese, A. Fantoni, G. Gervino, H. A. Gimm, P. Levi Sandri, L. Mazzaschi, V. Mokeev, V. Muccifora, E. Polli, A. R. Reolon, G. Ricco, M. Ripani, M. Sanzone, M. Taiuti, G. M. Urciuoli, and A. Zucchiatti, Phys. Rev. C **47**, R922 (1993).

[3] M. Anghinolfi, N. Bianchi, P. Corvisiero, A. Deppman, E. De Sanctis, A. Ebolese, A. Fantoni, G. Gervino, P. Levi Sandri, V. Lucherini, L. Mazzaschi, V. Mokeev, V. Muccifora, E. Polli, A. R. Reolon, G. Ricco, M. Ripani, P. Rossi, M. Sanzone, M. Taiuti, and A. Zucchiatti, Nucl. Phys. A **553**, 631 (1993).

[4] N. Bianchi, V. Muccifora, A. Deppman, E. De Sanctis, A. Fantoni, P. Levi Sandri, V. Lucherini, M. Mirazita, E. Polli, A. R. Reolon, P. Rossi, M. Anghinolfi, P. Corvisiero, G. Gervino, L. Mazzaschi, V. Mokeev, G. Ricco, M. Ripani, M. Sanzone, M. Taiuti, and A. Zucchiatti, Phys. Lett. B **309**, 5 (1993).

[5] N. Bianchi, E. De Sanctis, M. Mirazita, and V. Muccifora, Phys. Rev. C **60**, 064617 (1999).

[6] M. Gonçalves, E. C. de Oliveira, E. L. Medeiros, S. de Pina, and S. B. Duarte, Braz. J. Phys. **34**, 919 (2004).

[7] J. J. Sakurai, Phys. Rev. Lett. **22**, 981 (1969).

[8] A. Baracca and A. Bramón, Nuovo Cimento A **69**, 613 (1970).

[9] S. J. Brodsky, L. Frankfurt, J. F. Gunion, A. H. Mueller, and M. Strikman, Phys. Rev. D **50**, 3134 (1994).

[10] J. C. Collins, L. Frankfurt, and M. Strikman, Phys. Rev. D **56**, 2982 (1997).

[11] A. J. Baltz, G. Baur, D. d'Enterria, L. Frankfurt, F. Gelis, V. Guzey, K. Hencken, Yu. Kharlov, M. Klasen, S. R. Klein, V. Nikulin, J. Nystrand, I. A. Pshenichnov, S. Sadovsky, E. Scapparone, J. Seger, M. Strikman, M. Tverskoy, R. Vogt, S. N. White, U. A. Wiedemann, P. Yepes, and M. Zhalov, Phys. Rep. **458**, 1 (2008).

[12] E. Abbas *et al.* (ALICE Collaboration), Eur. Phys. J. C **73**, 2617 (2013).

[13] I. A. Pshenichnov, I. N. Mishustin, J. P. Bondorf, A. S. Botvina, and A. S. Iljinov, Phys. Rev. C **60**, 044901 (1999).

[14] G. S. dos Santos and M. V. T. Machado, Phys. Rev. C **89**, 025201 (2014).

[15] M. H. Wood *et al.* (CLAS Collaboration), Int. J. Mod. Phys. A **26**, 734 (2011).

[16] P. Eugenio *et al.* (CLAS Collaboration), in *11th Conference on the Intersections of Particles and Nuclear Physics (CIPANP)*, St. Petersburg, 2012, edited by B. Fleming, AIP Conf. Proc. No. 1560 (AIP, New York, 2013), p. 421.

[17] M. H. Wood *et al.* (CLAS Collaboration), Phys. Rev. C **78**, 015201 (2008).

[18] C. Djalali, M. Paolone, D. Weygand, M. H. Wood, and R. Nasseripour, in *The IX International Conference on Quark Confinement and the Hadron Spectrum–QCHS IX*, Madrid, 2010, edited by F. J. Llanes-Estrada and J. R. Pelàez, AIP Conf. Proc. No. 1343 (AIP, New York, 2011), p. 574.

[19] H. W. Bertini, Phys. Rev. **188**, 1711 (1969).

[20] Y. Yariv and Z. Fraenkel, Phys. Rev. C **20**, 2227 (1979).

[21] Y. Yariv and Z. Fraenkel, Phys. Rev. C **24**, 488 (1981).

[22] V. S. Barashenkov [in Russian], JINR Report No. JINR P2-81-364, Dubna, 1981 (unpublished).

[23] V. S. Barashenkov and V. D. Toneev, *Interaction of High Energy Particles and Nuclei with Atomic Nuclei* (Atomizdat, Moscow, 1972), in Russian.

[24] V. S. Barashenkov, A. S. Ilinov, N. M. Sobolevskii, and V. D. Toneev, Usp. Fiz. Nauk **109**, 91 (1973) [Sov. Phys. Usp. **16**, 31 (1973)].

[25] V. S. Barashenkov, Van Ngok Le, L. G. Levchuk, Zh. Zh. Musulmanbekov, and A. N. Sosnin *et al.*, JINR Report No. JINR P2-85-173, Dubna, 1985 (unpublished).

[26] I. A. Pshenichnov, I. N. Mishustin, J. P. Bondorf, A. S. Botvina, and A. S. Iljinov, Phys. Rev. C **57**, 1920 (1998).

[27] I. A. Pshenichnov, B. L. Berman, W. J. Briscoe, C. Cetina, G. Feldman, P. Heimberg, A. S. Iljinov, and I. I. Strakovsky, Eur. Phys. J A **24**, 69 (2005).

[28] P. Golubev, V. Avdeichikov, K. G. Fissum, B. Jakobsson, I. A. Pshenichnov, W. J. Briscoe, G. V. O'Rielly, J. Annand, K. Hansen, L. Isaksson, H. Jäderström, M. Karlsson, M. Lundin, B. Schröder, and L. Westerberg, Nucl. Phys. A **806**, 216 (2008).

[29] I. A. Pshenichnov, Phys. Part. Nuclei **42**, 1063 (2011).

[30] Y. Malyshkin, I. A. Pshenichnov, I. Mishustin, and W. Greiner, Phys. Rev. C **78**, 015201 (2012).

[31] E. V. Karpechev, I. A. Pshenichnov, and T. L. Karavicheva *et al.*, Nucl. Phys. A **921**, 60 (2014).

[32] A. S. Iljinov, I. A. Pshenichnov, N. Bianchi, E. De Sanctis, V. Muccifora, M. Mirazita, and P. Rossi, Nucl. Phys. A **616**, 575 (1997).

[33] K. K. Gudima and S. G. Mashnik, in Proceedings of the 11th International Conference on Nuclear Reaction Mechanisms, Varenna, Italy, June 2006, Report No. LA-UR-06-4693, Los Alamos, 2006 (unpublished), pp. 525–534.

[34] S. G. Mashnik, M. I. Baznat, K. K. Gudima, A. J. Sierk, and R. E. Prael, Report No. LA-UR-05-2013, Los Alamos, 2005 (unpublished).

[35] A. Boudard, J. Cugnon, S. Leray, and C. Volant, Phys. Rev. C **66**, 044615 (2002).

[36] J. Cugnon, C. Volant, and S. Vuillier, Nucl. Phys. A **620**, 475 (1997).

[37] M. Gonçalves, S. de Pina, D. A. Lima, W. Milomen, E. L. Medeiros, and S. B. Duarte, Phys. Lett. B **406**, 1 (1997).

[38] A. Boudard, J. Cugnon, J.-C. David, S. Leray, and D. Mancusi, Phys. Rev. C **87**, 014606 (2013).

[39] A. Deppman, G. Silva, S. Anéfalos, S. B. Duarte, F. García, F. H. Hisamoto, and O. A. P. Tavares, Phys. Rev. C **73**, 064607 (2006).

[40] S. A. Pereira, A. Deppman, G. Silva, J. R. Maiorino, A. dos Santos, S. B. Duarte, O. A. P. Tavares, and F. Garcia, EPJ Web Conf. **21**, 10001 (2012).

[41] A. Deppman, S. B. Duarte, G. Silva, O. A. P. Tavares, S. Anéfalos, J. D. T. Arruda-Neto, and T. E. Rodrigues, J. Phys. G: Nucl. Part. Phys. **30**, 1991 (2004).

[42] T. Kodama, S. B. Duarte, K. C. Chung, and R. A. M. S. Nazareth, Phys. Rev. Lett. **49**, 536 (1982).

[43] B. D. Serot and J. D. Walecka, Adv. Nucl. Phys. **16**, 1 (1986).

[44] E. Andrade-II, J. C. M. Menezes, S. B. Duarte, F. Garcia, P. C. R. Rossi, O. A. P. Tavares, and A. Deppman, J. Phys. G: Nucl. Part. Phys. **38**, 085104 (2011).

[45] A. Deppman, O. A. P. Tavares, S. B. Duarte, J. D. T. Arruda-Neto, M. Gonçalves, V. P. Likhachev, and E. C. de Oliveira, Phys. Rev. C **66**, 067601 (2002).

[46] E. Andrade-II, E. Freitas, and O. A. P. Tavares *et al.*, in *Nuclear Physics 2008: XXXI Workshop on Nuclear Physics in Brazil*, São Paulo, September 2008, edited by V. Guimaraes, J. R. B. Oliveira, K. C. D. Macario, and F. A. Genezini, AIP Conf. Proc. No. 1139 (AIP, New York, 2009), p. 64.

[47] V. P. Likhachev, J. Mesa, J. D. T. Arruda-Neto, B. V. Carlson, W. R. Carvalho, Jr., L. C. Chamon, A. Deppman, H. Dias, and M. S. Hussein, Nucl. Phys. A **713**, 24 (2003).

[48] V. P. Likhachev, J. D. T. Arruda-Neto, W. R. Carvalho, A. Deppman, I. G. Evseev, F. Garcia, M. S. Hussein, L. F. R. Macedo, A. Margaryan, J. Mesa, V. O. Nesterenko, O. Rodriguez, S. A. Pashchuk, H. R. Schelin, and M. S. Vaudeluci, Phys. Rev. C **68**, 014615 (2003).

[49] S. de Pina, E. C. de Oliveira, E. L. Medeiros, S. B. Duarte, and M. Gonçalves, Phys. Lett. B **434**, 1 (1998).

[50] I. González, C. Barbero, A. Deppman, S. B. Duarte, F. Krmpotić, and O. Rodriguez, J. Phys. G: Nucl. Part. Phys. **38**, 115105 (2011).

[51] I. González, A. Deppman, S. B. Duarte, F. Krmpotić, M. S. Hussein, and C. Barbero, J. Phys.: Conf. Ser. **312**, 022017 (2011).

[52] F. Krmpotić, A. Deppman, and C. De Conti, in *Nuclear Structure and Dynamics 2012*, Opatija, Croatia, July 2012, edited by T. Nikšic, M. Milin, D. Vretenar, and S. Szilner, AIP Conf Proc. No. 1491 (AIP, New York, 2012), p. 1167.

[53] A. Deppman, O. A. P. Tavares, S. B. Duarte, E. C. de Oliveira, J. D. T. Arruda-Neto, S. R. de Pina, V. P. Likhachev, O. Rodriguez, J. Mesa, and M. Gonçalves, Phys. Rev. Lett. **87**, 182701 (2001).

[54] A. Deppman, O. A. P. Tavares, S. B. Duarte, J. D. T. Arruda-Neto, M. Gonçalves, V. P. Likhachev, J. Mesa, E. C. de Oliveira, S. R. de Pina, and O. Rodriguez, Nucl. Instrum. Methods Phys. Res. Sect. B **211**, 15 (2003).

[55] A. Deppman, O. A. P. Tavares, S. B. Duarte, E. C. de Oliveira, J. D. T. Arruda-Neto, S. R. de Pina, V. P. Likhachev, O. Rodriguez, J. Mesa, and M. Gonçalves, Comput. Phys. Commun. **145**, 385 (2002).

[56] A. Deppman, E. Andrade-II, V. Guimarães, G. S. Karapetyan, O. A. P. Tavares, A. R. Balabekyan, N. A. Demekhina, J. Adam, F. Garcia, and K. Katovsky, Phys. Rev. C **88**, 064609 (2013).

[57] E. Martynov, E. Predazzi, and A. Prokudin, Phys. Rev. D **67**, 074023 (2003).

[58] Marcel Froissart, Phys. Rev. **123**, 1053 (1961).

[59] E. Martynov, E. Predazzi, and A. Prokudin, Eur. Phys. J. C **26**, 271 (2002).

[60] S. Chekanov *et al.*, Eur. Phys. J. C **24**, 345 (2002).

[61] J. A. Crittenden, arXiv:hep-ex/9704009, Reports No. DESY-97-068 and No. BONN-IR-97-01, 1997 (unpublished).

[62] G. I. Lykasov, W. Cassing, A. Sibirtsev, and M. V. Rzjanin, Eur. Phys. J. A **6**, 71 (1999).

[63] M. Gell-Man, D. Sharp, and W. G. Wagner, Phys. Rev. Lett. **8**, 261 (1962).

[64] A. Sibirtsev, W. Cassing, G. I. Lykasov, and M. V. Rzjanin, Nucl. Phys. A **632**, 131 (1998).

[65] J. J. de Swart, M. C. M. Rentmeester, and R. G. E. Timmermans, π N Newsletter **13**, 96 (1997), Report No. THEF-NYM-97.1, KVI 1318, arXiv:nucl-th/9802084.

[66] I. Antcheva, M. Ballintijn, B. Bellenot, M. Biskup, and R. Brun *et al.*, Comput. Phys. Commun. **180**, 2499 (2009).

[67] F. James, Report No. CERN-68-15, 1968 (unpublished).

[68] A. Sibirtsev, K. Tsushima, and A. W. Thomas, Phys. Rev. C **63**, 044906 (2001).

[69] M. C. Abreu *et al.*, Phys. Lett. B **477**, 28 (2000).

[70] A. Sibirtsev, K. Tsushima, and A. W. Thomas, Eur. Phys. J. A **6**, 351 (1999).

[71] A. Sibirtsev, W. Cassing, and U. Mosel, Z. Phys. A **358**, 357 (1997).

[72] D. O. Caldwell, V. B. Elings, W. P. Hesse, G. E. Jahn, R. J. Morrison, F. V. Murphy, and D. E. Yount, Phys. Rev. Lett. **23**, 1256 (1969).

[73] D. O. Caldwell *et al.*, Phys. Rev. D **7**, 1362 (1973).

[74] S. J. Brodsky, Ivan Schmidt and Guy F. de Téramond, Phys. Rev. Lett. **64**, 1011 (1990).
[75] M. Effenberger, E. L. Bratkovskaya, W. Cassing, and U. Mosel, Phys. Rev. C **60**, 027601 (1999).
[76] R. Nasseripour *et al.* (CLAS Collaboration), Phys. Rev. Lett. **99**, 262302 (2007).
[77] M. Kotulla *et al.* (CBELSA/TAPS Collaboration), Phys. Rev. Lett. **100**, 192302 (2008).
[78] D. Cabrera, L. Roca, E. Oset, H. Toki, and M. J. Vicente Vacas, Nucl. Phys. A **733**, 130 (2004).
[79] P. Mühlich and U. Mosel, Nucl. Phys. A **765**, 188 (2006).
[80] P. Mühlich and U. Mosel, Nucl. Phys. A **773**, 156 (2006).
[81] T. Ishikawa *et al.*, Phys. Lett. B **608**, 215 (2005).
[82] Wood *et al.* (CLAS Collaboration), Phys. Rev. Lett. **105**, 112301 (2010).